THE JOURNAL OF BIOLOGICAL CHEMISTRY VOL. 283, NO. 48, pp. 33240–33248, November 28, 2008

Projection Structure of a Member of the Amino Acid/Polyamine/Organocation Transporter Superfamily*

Received for publication, September 8, 2008, and in revised form, September 18, 2008 Published, JBC Papers in Press, September 25, 2008, DOI 10.1074/jbc.M806917200

Fabio Casagrande[‡1], Merce Ratera[§1,2], Andreas D. Schenk[‡], Mohamed Chami[‡], Eva Valencia[§3], Jesus Maria Lopez[¶‖], David Torrents[¶], Andreas Engel[‡], Manuel Palacin[§4,5], and Dimitrios Fotiadis[‡‡4,6]**

*From the [‡]M. E. Müller Institute for Structural Biology, Biozentrum of the University of Basel, CH-4056 Basel, Switzerland, the [§]Institute for Research in Biomedicine, Barcelona Science Park, Department of Biochemistry and Molecular Biology, Faculty of Biology, University of Barcelona and Centro de Investigacion Biomedica en Red de Enfermedades Raras, E-08028 Barcelona, Spain, the [¶]Barcelona Supercomputing Center, Life Science Program, E-08034 Barcelona, Spain, the [‖]National Institute of Bioinformatics, E-08034 Barcelona, Spain, the **Institucio Catalana de Recerca i Estudis Avancats, E-08034 Barcelona, Spain, and the [‡‡]Institute for Biochemistry and Molecular Medicine of the University of Berne, CH-3012 Berne, Switzerland*

The L-arginine/agmatine antiporter AdiC is a key component of the arginine-dependent extreme acid resistance system of *Escherichia coli*. Phylogenetic analysis indicated that AdiC belongs to the amino acid/polyamine/organocation (APC) transporter superfamily having sequence identities of 15–17% to eukaryotic and human APC transporters. For functional and structural characterization, we cloned, overexpressed, and purified wild-type AdiC and the point mutant AdiC-W293L, which is unable to bind and consequently transport L-arginine. Purified detergent-solubilized AdiC particles were dimeric. Reconstitution experiments yielded two-dimensional crystals of AdiC-W293L diffracting beyond 6 Å resolution from which we determined the projection structure at 6.5 Å resolution. The projection map showed 10–12 density peaks per monomer and suggested mainly tilted helices with the exception of one distinct perpendicular membrane spanning α-helix. Comparison of AdiC-W293L with the projection map of the oxalate/formate antiporter from *Oxalobacter formigenes*, a member from the major facilitator superfamily, indicated different structures. Thus, two-dimensional crystals of AdiC-W293L yielded the first detailed view of a transport protein from the APC superfamily at sub-nanometer resolution.

Enteric pathogens such as *Shigella*, *Salmonella*, *Yersinia*, spp., and certain *Escherichia coli* strains can survive the extremely acidic conditions of the human stomach and cause intestinal diseases (1). To overcome the protective barrier of the gastric acidity, pathogenic and nonpathogenic strains of *E. coli* have developed acid resistance systems. One of these systems requires arginine to protect *E. coli* during low pH exposure. This arginine system is composed of an arginine-agmatine exchange transporter and of an acid-activated arginine decarboxylase (2). Acidification of the cytosol is prevented by the consumption of protons through decarboxylation of arginine to agmatine and carbon dioxide. Agmatine is then exported out of the cytosol, and new arginine is imported through the arginine-agmatine transporter in a one-to-one exchange stoichiometry (2). This recently identified transport protein is the product of the *adiC* gene (3, 4). *In vitro*, AdiC-mediated exchange transport of arginine and agmatine is tightly coupled, electrogenic, and acid-activated (5). AdiC forms stable homodimers in detergent and phospholipid membranes as determined by gel filtration and glutaraldehyde cross-linking experiments (5).

The origin of AdiC is somehow controversial as it was assigned to two families of transport proteins, *i.e.* the amino acid/polyamine/organocation (APC)[7] transporter superfamily (6) and the major facilitator superfamily (MFS) (5, 7). The APC superfamily of transporters consists of nearly 250 members that function as solute-cation symporters and solute-solute antiporters (6). According to hydropathy profile analysis and biochemically established topological features of most prokaryotic and eukaryotic APC superfamily members, both the N and C termini of the proteins are located in the cytoplasm with a 12-transmembrane segment topology (6, 8–11). Two subfamilies of the APC transporter superfamily, *i.e.* the cationic amino acid transporters (CATs) and the L-type amino acid transporters (LATs), have human members involved in relevant physiological functions and diseases. CAT2 provides arginine for NO

* This work was supported by the European Community Project Grant 502802 EUGINDAT (to D. F. and M. P.), by the Berne University Research Foundation (to D. F. and Matthias Hediger), by the Spanish Ministry of Science and Education Grant BFU2006-14600 (to M. P.), by the Swiss National Center of Competence in Research for Structural Biology (to A. E.), and by the Maurice E. Müller Foundation of Switzerland (to A. E.). The costs of publication of this article were defrayed in part by the payment of page charges. This article must therefore be hereby marked "*advertisement*" in accordance with 18 U.S.C. Section 1734 solely to indicate this fact.

[1] These two authors contributed equally to this work.
[2] Recipient of a pre-doctoral fellowship from the Spanish Ministry of Science and Education.
[3] Recipient of a Juan de La Cierva contract from the Spanish Ministry of Science and Education with support from the Fondo Social Europeo.
[4] These two authors share senior authorship.
[5] To whom correspondence may addressed: Institute for Research in Biomedicine, Barcelona Science Park, Josep Samitier 1-5, E-08028 Barcelona, Spain. Tel.: 34-93-403-7199; Fax: 34-93-403-4717; E-mail: manuel.palacin@irbbarcelona.org.
[6] To whom correspondence may addressed: Institute of Biochemistry and Molecular Medicine, University of Berne, Bühlstrasse 28, CH-3012 Berne, Switzerland. Tel.: 41-31-631-4103; Fax: 41-31-631-3737; E-mail: dimitrios.fotiadis@mci.unibe.ch.

[7] The abbreviations used are: APC, amino acid/polyamine/organocation; CAT, cationic amino acid transporters; MFS, major facilitator superfamily; LAT, L-type amino acid transporters; TEM, transmission electron microscopy; APA, amino acid/polyamine antiporter; ITC, isothermal titration calorimetry; DDM, *n*-dodecyl-β-D-maltopyranoside; OxlT, oxalate/formate antiporter from *O. formigenes*; BN, blue native.

synthesis (12) and for arginase (13) in classical and alternative activation of macrophages, and CAT1 is required for macrophage proliferation (14). LAT1 is overexpressed in a wide spectrum of primary human cancers and plays important roles in the growth and survival of cancer cell lines (15). Mutations in the human LAT members $b^{0,+}AT$ (and in its associated heavy subunit rBAT) and y^+LAT1 cause the primary inherited aminoacidurias cystinuria, and lysinuric protein intolerance, respectively (16–19). Another LAT transporter, xCT, is Kaposi sarcoma-associated herpesvirus fusion-entry receptor (20).

Structural information on amino acid transporters is sparse. Only two high resolution structures have been reported so far, that of the bacterial glutamate transporter Glt_{ph} (21) and that of the bacterial leucine transporter $LeuT_{Aa}$ (22). Thus, besides low resolution transmission electron microscopy (TEM) data on single detergent-solubilized Ser/Thr exchanger transport proteins (SteT) (23), no structural information is available for other members of the APC transporter superfamily. The low number of amino acid transporter structures and of membrane proteins in general is related to the difficulty in growing highly ordered three-dimensional membrane protein crystals for structure determination by x-ray crystallography. Cryo-TEM combined with electron crystallography of two-dimensional crystals to establish the three-dimensional protein structure is an attractive alternative to x-ray crystallography and three-dimensional crystals (24). An important advantage of two-dimensional membrane protein crystals is that the protein is embedded in its native environment, the lipid bilayer. Recently, the first two-dimensional crystals of an amino acid transporter, *i.e.* Glt_{ph}, have been reported (25).

Here we present for the first time structural data at subnanometer resolution of the L-arginine/agmatine antiporter AdiC. Phylogenetic analysis indicated that AdiC belongs to the APC superfamily and not to the MFS. This assignment was further supported by the different projection structure of AdiC, as obtained by cryo-TEM of two-dimensional crystals, compared with that of the oxalate/formate antiporter from *Oxalobacter formigenes*, a typical member from the MFS. To grow two-dimensional crystals, we overexpressed AdiC and the mutant AdiC-W293L in *E. coli* and purified both forms to homogeneity. Negative-stain TEM and blue native-polyacrylamide gel electrophoresis (BN-PAGE) of both detergent-solubilized AdiC proteins revealed a homodimeric state. Reconstitution experiments yielded first well ordered two-dimensional crystals of AdiC-W293L suitable for structure analysis by cryo-TEM. The projection map calculated from unstained two-dimensional crystals revealed the structure of AdiC-W293L at 6.5 Å resolution. The present work sets the basis for the structural analysis of AdiC at high resolution using two-dimensional crystals and cryo-TEM/electron crystallography. Importantly, AdiC represents an excellent model for understanding the molecular architecture of transporters from the APC superfamily.

EXPERIMENTAL PROCEDURES

Chemicals—E. coli polar lipids were purchased from Avanti Polar Lipids (Alabaster, AL) and *n*-dodecyl-β-D-maltopyranoside (DDM) from Anatrace (Maumee, OH). Radiolabeled L-[^{3}H]Arginine was from American Radiolabeled Chemicals (St. Louis, MO), and amino acids and amines were from Sigma-Aldrich.

Phylogenetic Analysis of AdiC—Comparative searches of the AdiC gene (National Center for Biotechnology Information (NCBI) GenInfo (gi): 16131941) were performed using the BLAST algorithm (www.ncbi.nlm.nih.gov/blast) against the default nr protein data base (GenBank^{TM} CDS translations + RefSeq Proteins + PDB + SwissProt + PIR + PRF) and using default parameters. To build the phylogenetic tree, we first performed a multiple alignment using PROBCONS (26) with the AdiC protein sequence and other protein sequences collected from NCBI and the TCDB Transport Classification Database (6) that are representatives of the following APC subfamilies: amino acid/polyamine antiporter (APA) (PotE/gi: 26246666 from *E. coli*; CadB/gi: 536977 from *E. coli*; ArcD/gi: 254827 from *Pseudomonas aeruginosa*; LysI/gi: 38233510 from *Corynebacterium glutamicum*; YvsH/gi: 16080387 from *Bacillus subtilis*), ACT (GabA/gi: 4972245 from *Emericella nidulans* and Uga4/gi: 6319991 from *Saccharomyces cerevisiae*), CAT (CAT1/gi: 161016790 from *Mus musculus*; CAT2/gi: 113680130 from *M. musculus*; AAT1/gi: 30685317 from *Arabidopsis thaliana*; YfnA/gi: 16077801 from *B. subtilis*), GGA (XasA/gi: 33241625 from *Chlamydophila pneumoniae*), AGT (yveA/gi: 16080500 from *B. subtilis*; ybeC/gi: 16077281 from *B. subtilis*), and LAT (SteT/gi: 16078351 from *B. subtilis* and eukaryotic LATs: LAT2/gi: 33286428 from *Homo sapiens*, LAT1/gi: 71979932 from *H. sapiens*, y^+LAT1/gi: 21361563 from *H. sapiens*), and $b^{0,+}AT$ from *Monodelphis domestica* (ENMSEBL:ENSMODP00000015349), from *Canis familiaris* (ENMSEBL:ENSCAFP00000011140), and from *Rattus norvegicus* (ENMSEBL:ENSRNOP00000016919). As outgroup for the tree, we selected Mmup/gi: 172051482 of *E. coli* that belongs to the AAT family. We next evaluated this alignment and obtained the tree using the Bayesian phylogenetic method (27) (GTR model, 5 million generations and excluding 40% of the initial trees). The tree was elaborated and prepared for proper display with the iTOL online tool (28).

Cloning, Mutagenesis, and Overexpression of AdiC and AdiC-W293L—AdiC was cloned from genomic *E. coli* strain DH5α DNA as previously described for other transporters (23). Briefly, the following primers (5′-3′) were used to amplify the AdiC open reading frame by PCR: ATGAGAATTCACTATCGAATGCAGGCGTATG and TCATCTCGAGGTTGGCTTTTATGTTTGCTGGA. PCR products were digested with EcoRI and XhoI and ligated into a pBlueScript vector (Stratagene, La Jolla, CA). Another PCR with the following primers (5′-3′) was performed to subclone the AdiC open reading frame into the EcoRI and PstI sites of a modified version of the vector pTTQ18 (29), thereby placing its expression under the control of the *tac* promoter: TGATGAATTCGATGTCTTCGGATGCTGATGC and ACCGCCTGCAGAATCTTTGCTTATTGGTGCA. Mutation W293L in AdiC was introduced in AdiC cloned into pTTQ18 using QuikChange site-directed mutagenesis kit (Stratagene) with primer (5′-3′) GCTTAGGTTCACTGGGCGGCT(T)GACGTTGCTGGCGGGTC and its complementary reverse primer. For isothermal titration calorimetry (ITC) studies AdiC was amplified from the pBlueScript con-

struct using as primers (5′-3′) CAATGGATCCATGTCTTC-GGATGCTGATGCTC and TCATCTCGAGGTTGGCTTT-TATGTTTGCTGGA and subcloned into BamHI and XhoI sites of the pTrcHisA vector. All DNA constructs were verified by sequencing. Expression experiments were carried out with freshly transformed *E. coli* BL21(DE3) harboring pTTQ18-His_6-AdiC, pTTQ18-His_6-AdiC-W293L, or pTrcHisA-AdiC. In cultures grown in LB medium, optimal expression of the AdiC proteins occurred after 3 h at 37 °C after induction at A_{600} of 0.5 with 0.5 mM isopropyl-β-D-thiogalactoside. Routinely, four to six liters of medium in flasks were inoculated with the corresponding AdiC construct, and after 3 h of growth at 37 °C, cells were harvested. Cell pellets were resuspended in lysis buffer (20 mM Tris-HCl, pH 8.0, 0.5 mM EDTA).

Preparation of E. coli Membranes—Cell pellets were disrupted by passage through a French pressure cell (20,000 p.s.i.). Unbroken cells were removed by centrifugation (10 min at 10,000 × *g*, 4 °C). The supernatant was ultracentrifuged (1 h at 100,000 × *g*, 4 °C), and the pellet was resuspended and homogenized (30-ml glass homogenizer) in lysis buffer and ultracentrifuged again. Peripheral membrane proteins were removed by homogenization in 20 mM Tris-HCl, pH 8.0, 300 mM NaCl and ultracentrifugation. Finally, the membrane pellet was resuspended in 20 mM Tris-HCl pH 8.0, 150 mM NaCl at a protein concentration between 13 and 25 mg/ml. Aliquots were frozen in liquid nitrogen and stored at −80 °C until use.

Purification of AdiC and AdiC-W293L and Determination of Protein Concentration—Frozen *E. coli* total membranes containing overexpressed AdiC or AdiC-W293L were thawed and solubilized for 2 h at 4 °C under gentle agitation in 1% DDM, 20 mM Tris-HCl, pH 8, 300 mM NaCl, 10% glycerol, 0.01% NaN_3. The protein concentration during solubilization was between 2 and 3 mg/ml. After ultracentrifugation (100,000 × *g*, 50 min at 4 °C) the supernatant was diluted 2-fold with 20 mM Tris-HCl, pH 8, 300 mM NaCl, 0.04% DDM, 5 mM histidine, 10% glycerol, 0.01% NaN_3 (washing buffer) and bound for 2 h at 4 °C to nickel-nitrilotriacetic acid Superflow beads (Qiagen, Hilden, Germany). The beads were then loaded onto a spin column (Promega, Madison, WI), washed with washing buffer, and eluted with the same buffer containing 200 mM histidine. For ITC studies protein bound beads were washed twice with 20 mM imidazole in 20 mM Tris-HCl, pH 7.6, 150 mM NaCl, 0.01% DDM. AdiC-W293L was eluted with 300 mM imidazole in the same buffer. Untagged AdiC was eluted by overnight digestion at room temperature with enterokinase (Invitrogen) (5 units/mg of protein) in 20 mM Tris-HCl, pH 7.6, 10 mM $CaCl_2$, and 0.01% DDM. Then protein was further purified by size-exclusion chromatography using a Superdex 200 (10/300) column (GE Healthcare) and concentrated with Vivaspin MWCO100 (Sigma-Aldrich). Protein concentration was determined spectrophotometrically measuring the absorbance at 280 nm and using a molar extinction coefficient of 85,830 M^{-1} cm^{-1} (His-tagged AdiC), 91,830 M^{-1} cm^{-1} (untagged AdiC), and 80,330 M^{-1} cm^{-1} (His-tagged AdiC-W293L). These values were calculated from the amino acid sequence of the different AdiC versions using the ProtParam tool from the ExPASy proteomics server.

Transport Measurements—For functional studies, purified AdiC proteins were reconstituted into proteoliposomes as previously described (23). L-[^{3}H]Arginine influx measurements into AdiC and AdiC-W293L proteoliposomes were performed according to Reig *et al.* (23). All experimental values were corrected by subtracting zero time values and are reported as the means ± S.E.

ITC—All solutions were degassed before titration in an ITC instrument (MicroCal). A solution of AdiC or AdiC-W293L (0.1 mM in 1.4 ml of buffer (20 mM Tris-HCl, pH 7.5, 150 mM NaCl, 0.01% DDM)) was loaded into the sample cell, 2.5 mM titrant L-arginine in the same buffer was loaded into the injection syringe, and the system was equilibrated at 25 °C. Titration curves were generated by 30 successive 10-μl injections at 240-s intervals. ITC performed with two independent preparations of AdiC and AdiC-W293L gave very similar results. Control injections were performed in the absence of protein to determine background corrections due to substrate dilution. The data were fitted to a Single Set of Identical Sites Model with the Origin software (OriginLab).

Two-dimensional Crystallization of AdiC—Purified AdiC and AdiC-W293L protein solubilized in DDM was mixed with *E. coli* polar lipids solubilized in the same detergent (stock solution: 5 mg/ml *E. coli* polar lipids, 1% DDM, 20 mM Tris-HCl, pH 8, 150 mM NaCl, 10% glycerol, 0.01% NaN_3) to achieve a lipid-to-protein ratio of 0.3 (w/w). The final AdiC/AdiC-W293L protein concentration was adjusted to about 1 mg/ml. The protein/lipid/detergent mix was dialyzed against detergent-free buffer, *i.e.* 20 mM citric acid-NaOH, pH 5, 250 mM NaCl, 10% glycerol, 0.01% NaN_3, 5 mM L-arginine for about 2 weeks at room temperature.

Blue Native Gel Electrophoresis—Linear 5–12% gradient gels for BN-PAGE were prepared and run as previously described (30). Thyroglobulin (669 kDa), ferritin (440 kDa), lactate dehydrogenase (140 kDa), and bovine serum albumin (66 kDa) were used as standard proteins.

Negative Stain TEM—DDM-solubilized AdiC or AdiC-W293L protein at ~3 μg/ml was adsorbed for ~10 s to Parlodion carbon-coated copper grids rendered hydrophilic by glow discharge at low pressure in air. Grids were washed with three drops of double-distilled water and stained with 2 drops of 0.75% uranyl formate. Grids of negatively stained two-dimensional AdiC-W293L crystals (Fig. 5) were prepared similarly but included a longer adsorption time of ~60 s. Electron micrographs were recorded at a magnification of 50,000× on Eastman Kodak Co. SO-163 sheet films with a Hitachi H-7000 electron microscope operated at 100 kV.

Cryo-TEM—Two-dimensional crystals of AdiC-W293L were adsorbed to a thin carbon film on a molybdenum grid and frozen in liquid nitrogen in the presence of 7% (w/v) trehalose (31). Frozen grids were transferred into a Philips CM200-FEG electron microscope using a Gatan 626 cryo-holder. Electron micrographs were recorded on Eastman Kodak Co. SO-163 films at an accelerating voltage of 200 kV, a magnification of 50,000× using a low-dose system (~10 electrons per $Å^2$), and a measured specimen temperature of about −175 °C. The range of defocus values used was between 5,300 and 11,600 Å.

Image Processing—Electron micrographs of selected AdiC-W293L crystals were scanned using a Heidelberg Primescan D7100 scanner with a sampling of 1 Å/pixel at the sample level. The images were processed using the IPLT image processing toolkit (32, 33) to correct for the contrast transfer function and crystal distortions. The parameters of the contrast transfer function and the crystal lattice were fitted manually using the graphical user interface provided by IPLT. The five best images were scaled using one image as reference and merged to produce the final data set from which the projection represented as a contour map was generated within IPLT. No B-factor was used to sharpen the data. The plane group symmetry was determined using ALLSPACE (34). To generate the improved projection map of AdiC-W293L (Fig. 6*B*), one of the four identical AdiC-W293L dimers in the unit cell was symmetrized with IPLT exploiting the internal, non-crystallographic 2-fold symmetry axis of the dimer.

RESULTS

Phylogenetic Analysis of AdiC—The origin and evolution of the AdiC protein appears to be controversial, as it has been reported to belong to two distant groups of membrane transporters: MFS (5, 7) and the APC superfamily (6). To clarify this issue, we have analyzed *de novo* the phylogenetic relationship of AdiC with known transport proteins. We have combined two rounds of computational searches and comparisons with different levels of sensitivities and accuracies (see the "Experimental Procedures"). As an initial and rough approximation, we first used BLAST to compare the AdiC protein sequence against a non-redundant protein sequence data base and observed that the closest matches (other than predicted, potential, or hypothetical) were prokaryotic amino acid/polyamine antiporters, *e.g.* the proteins with the gi values of 152969070, 44886079, 10801580, and 123443711 (PotE) at the NCBI data base. These transporters belong to the basic APA family, a subgroup of the APC superfamily (6, 23). Next, and similar to our previous work with SteT (23), we selected a number of protein sequences representing APC subfamilies that are close to APA and calculated a Bayesian tree. As seen in Fig. 1, the tree indicated that AdiC clearly clusters with members of the APA family. In addition, the phylogenetic analysis revealed that eukaryotic and human APC transporters closest related to AdiC are members from the LAT family, *e.g.* xCT, y^+LAT1, and $b^{0,+}$AT, with sequence identities of 15–17%.

Cloning, Expression, and Purification of AdiC and AdiC-W293L—The AdiC gene from *E. coli* was amplified from genomic DNA by PCR using gene-specific primers. The W293L point mutation was introduced to diminish the number of possible conformations of AdiC and, thus, foster crystallization. The corresponding substitution (W292L) in the related APA transporter PotE (putrescine/ornithine exchanger from *E. coli*) results in an inactive transporter (35). For homologous overexpression, the AdiC and AdiC-W293L genes were cloned into the pTTQ18 vector fused with a C-terminal His_6 tag. Isolated *E. coli* total membranes containing overexpressed AdiC or AdiC-W293L were solubilized with DDM, and the corresponding protein was purified in a single step by nickel affinity chromatography. The high purity of the isolated proteins is reflected

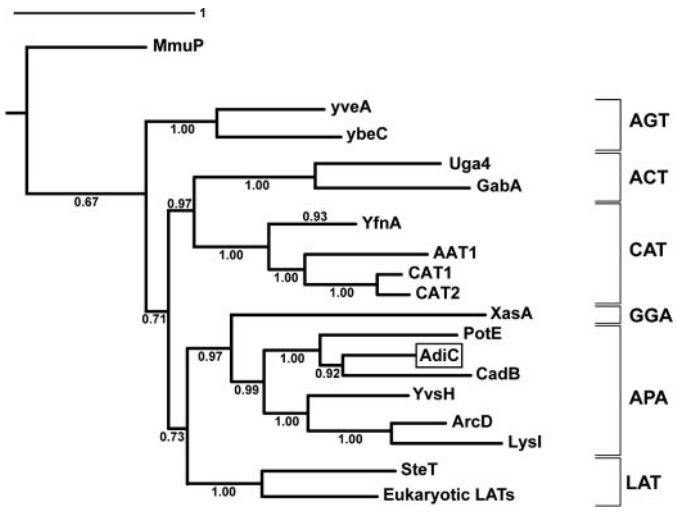

FIGURE 1. **Origin and evolutionary relationship of AdiC with other APC transport proteins.** The Bayesian tree shows the position of the AdiC protein sequence (within a *box*) in the context of other members of the APC transporter superfamily. The abbreviation of each of the subfamilies is on the *right side of the tree*: see Jack *et al.* (6) and TCDB Transport Classification Database for a description of each of the subfamilies displayed. The tree was rooted using the MmuP protein of *E. coli*. Probabilities given by Bayesian analysis are displayed at each of the tree nodes. The *bar* shows the evolutionary distance in number of expected substitutions per site.

in the SDS/polyacrylamide gels: AdiC (Fig. 2*A*, *lane 2*) and AdiC-W293L (Fig. 2*C*, *lane 2*). Both proteins run at ~39 kDa by SDS-PAGE. This was further confirmed by Western blot analysis using an anti-His antibody (data not shown). Because of the high expression levels, both AdiC forms were also visible in the DDM-solubilized *E. coli* total membranes: AdiC (Fig. 2*A*, *lane 1*) and AdiC-W293L (Fig. 2*C*, *lane 1*); see band at ~39 kDa. Typically, about 3 and 1 mg of pure AdiC and AdiC-W293L protein, respectively, were purified from 1 liter of bacterial cell culture.

Characterization of Purified AdiC and AdiC-W293L by BN-PAGE and Negative-stain TEM—To determine whether AdiC exists in a monomeric or oligomeric state, detergent-solubilized protein was subjected to BN-PAGE and negative stain TEM. On BN-gels, purified AdiC (Fig. 2*B*) and AdiC-W293L (Fig. 2*D*) migrated as single bands between 140 and 160 kDa depending on the experimental conditions. Denaturation of AdiC with SDS before BN-PAGE resulted in an additional band at ~70 kDa (data not shown). To assess the shape, dimensions, and low resolution structure of purified AdiC and AdiC-W293L, proteins were adsorbed on Parlodion carbon-coated grids, washed, negatively stained, and examined by TEM. Fig. 3*A* shows the high homogeneity of AdiC after purification by nickel affinity chromatography. Single AdiC particles were discerned and displayed an elliptical shape with a major axis of 121 ± 7 Å and a minor axis of 76 ± 6 Å ($n = 100$). The elongated particles had a dimeric appearance comparable with two connected ring-like structures. The central, stain-filled indentation in each ring was clearly visible on AdiC top views (Fig. 3*B*, gallery). As documented in Fig. 3*C*, AdiC-W293L had similar dimensions and appearance as AdiC.

Transport, Inhibition Pattern, and Substrate Binding in AdiC and AdiC-W293L—Transport of L-arginine via AdiC reconstituted in proteoliposomes is characteristic of an obligatory

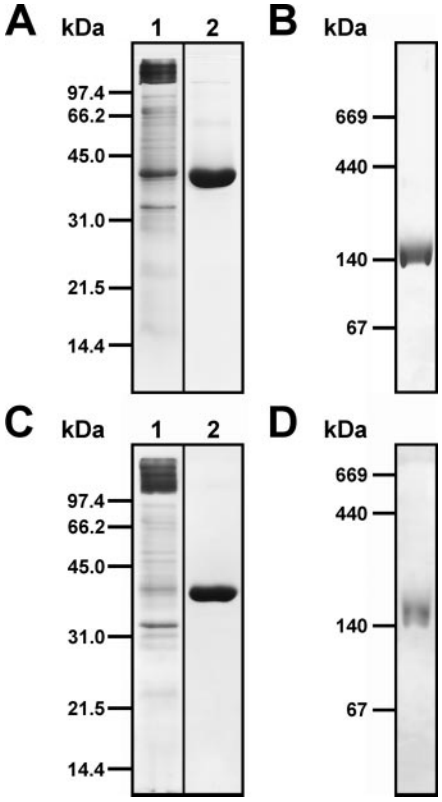

FIGURE 2. **SDS- and BN-PAGE of AdiC and AdiC-W293L.** *A*, 13.5% SDS-PAGE of DDM-solubilized *E. coli* total membranes containing overexpressed AdiC protein (*lane 1*) and of purified protein after nickel affinity chromatography (*lane 2*). AdiC runs as a prominent band at ~39 kDa in SDS/polyacrylamide gels. *B*, BN-PAGE of purified AdiC protein in a linear 5–12% gradient gel. *C*, same as in *A*, but for AdiC-W293L. *D*, same as in *B*, but for AdiC-W293L. All gels were stained with Coomassie Brilliant Blue R-250. Applied amount of protein per lane: ~9 μg (*lane 1*, *panel A*), ~6 μg (*lane 2*, *panel A*), ~12 μg (*panel B*), ~8 μg (*lane 1*, *panel C*), ~5 μg (*lane 2*, *panel C*), and ~5 μg (*panel D*).

exchanger. Thus, transport is dependent on the presence of substrate (L-arginine) inside AdiC proteoliposomes (Fig. 4*A*). In the absence of substrate inside, AdiC proteoliposome influx of L-[^{3}H]arginine most probably occurs by simple diffusion (Fig. 4*A*). Thus, this transport is very low and similar to that of L-serine with SteT (the LAT exchanger of Ser/Thr from *B. subtilis*) proteoliposomes under similar conditions (23). The exchange L-[^{3}H]arginine/L-arginine has a larger flux than the exchange L-[^{3}H]arginine/agmatine (Fig. 4*B*), in agreement with previous results (5). The inhibition profiles of L-[^{3}H]arginine/L-arginine exchange by 5 mM substrate analogs suggest the following affinity pattern: L-arginine, agmatine > cadaverine > putrescine > L-lysine, L-ornithine, L-glutamate, 1,3-diaminopropane > L-glutamine, aminoguanidine (Fig. 4*C*). This is in agreement with the previously reported transport competence profile for reconstituted AdiC: L-arginine > cadaverine > L-lysine, L-ornithine (5). Moreover, our results indicate that substitution of the agmatine guanidine group by amine is recognized by AdiC depending on the size of the aliphatic chain (Fig. 4*C*; cadaverine > putrescine > 1,3-diaminopropane).

AdiC-W293L proteoliposomes showed no L-[^{3}H]arginine/L-arginine exchange (Fig. 4*B*, *right*). Similarly, another AdiC point mutant involving the same residue, *i.e.* AdiC-W293C, could be expressed but was, as AdiC-W293L, inactive (data not shown).

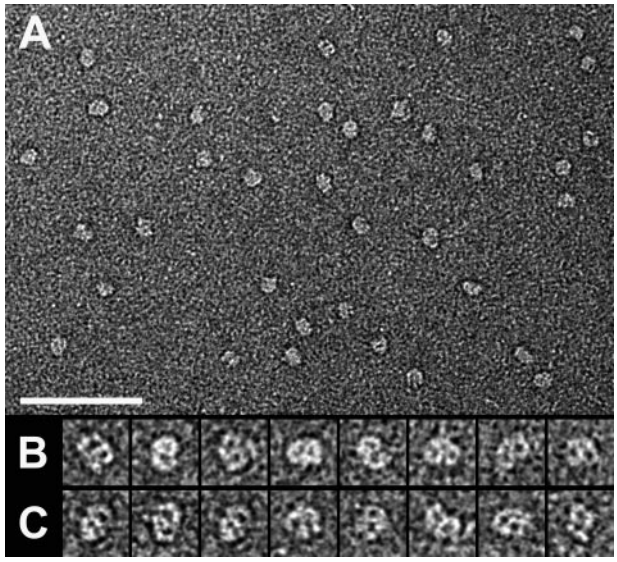

FIGURE 3. **TEM of negatively stained AdiC and AdiC-W293L particles.** *A*, the homogeneity of the purified AdiC protein is reflected in the electron micrograph. Selected top views of AdiC (*B*) and AdiC-W293L particles (*C*) are displayed in the corresponding gallery. The *scale bar* represents 750 Å, and the frame size of the magnified particles in the galleries is 190 Å.

To dissect whether the W293L mutation disrupts substrate recognition or translocation, substrate binding to AdiC-W293L in detergent solution was analyzed by ITC. AdiC without the His tag, with full exchange activity (data not shown), was used as a control in these studies. In agreement with a previous report using untagged AdiC (5) L-arginine titration produced signals of heat absorption, showing that binding is enthalpically unfavorable (ΔH^o = 1.5 kcal/mol) and, thus, entropy-driven (ΔS^o = 24 cal/(mol·K)) (data not shown). The calorimetric data were fitted to a Single Set of Identical Sites Model that indicated one substrate binding site per AdiC monomer, *i.e. n*, number of interaction sites = 0.96, with an equilibrium dissociation constant of 95 μM (data not shown). In contrast, AdiC-W293L showed no measurable heat absorption or production upon L-arginine titration (data not shown). This indicates the inability of AdiC-W293L to bind substrate.

Two-dimensional Crystallization and Projection Structure of AdiC-W293L—Purified AdiC and AdiC-W293L protein was reconstituted into lipid bilayers as described under "Experimental Procedures." Both AdiC proteins yielded tubular two-dimensional crystals diffracting better than 20 Å by negative stain (data not shown). However, AdiC-W293L crystals, in contrast to AdiC, diffracted significantly better by cryo-TEM and were, importantly, much more reproducible. Therefore, we focused on the determination of the projection structure of AdiC-W293L. Fig. 5*A* shows typical two-dimensional crystals of AdiC-W293L, measuring 0.4–0.6 μm in width and up to 2 μm in length. The lattice lines of such two-dimensional crystals are barely visible on noisy electron micrographs (Fig. 5*B*). Upon adsorption on carbon film, tubular crystals became flattened into two layers, one usually diffracting better than the other in the cryo-TEM. The best micrographs from cryo-TEM displayed reflections beyond 6 Å resolution (Table 1).

A 6.5 Å projection density map of AdiC-W293L was calculated by merging the data from five images (Fig. 6*A*; see also

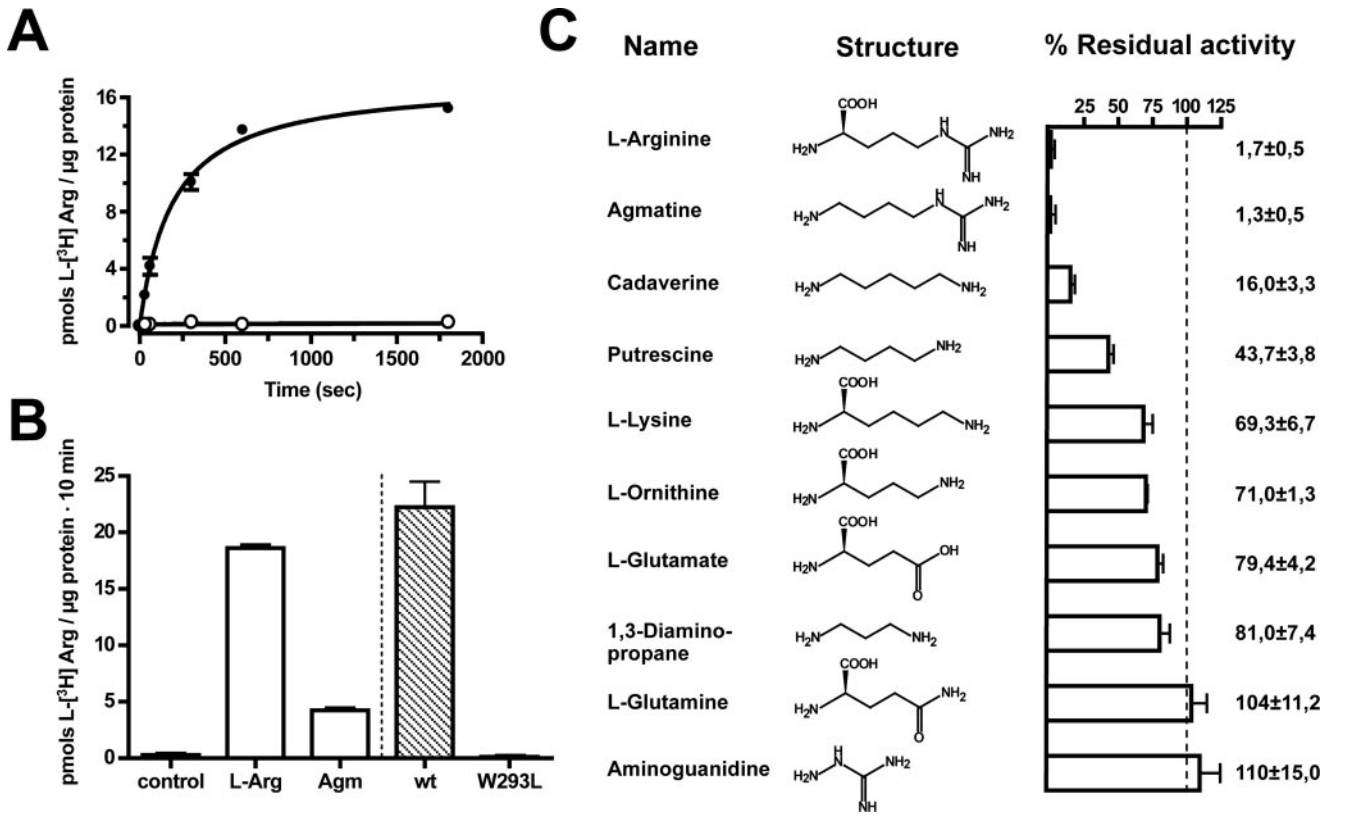

FIGURE 4. **AdiC transport activity.** *A*, time course of L-arginine transport in AdiC proteoliposomes. Influx of 10 μM L-[^{3}H]arginine into AdiC proteoliposomes lacking (*open circles*) or containing 2 mM L-arginine (*closed circles*). Data (mean ± S.E.) correspond to a representative experiment with three replicas. *Error bars* when not visible are smaller than symbols. *B*, influx of 10 μM L-[^{3}H]arginine into AdiC and AdiC-W293L proteoliposomes. Transport was measured in AdiC proteoliposomes (*left*) containing no substrate (*control*), 2 mM L-Arg, or 2 mM agmatine (*Agm*). Exchange activity in AdiC (wt) and AdiC-W293L (W293L) proteoliposomes (*right*) was calculated by subtracting transport in the corresponding proteoliposomes with no substrate inside to that in proteoliposomes containing 2 mM L-arginine. Data (mean ± S.E.) correspond to a representative experiment with three replicas. A second experiment gave similar results. *C*, inhibition pattern of AdiC transport in proteoliposomes. The residual exchange activity of 10 μM L-[^{3}H]arginine (outside) and 2 mM L-arginine (inside) in the presence of the indicated substrate analogs (5 mM) in the external medium is shown. Exchange activity was calculated as in *panel B* and is expressed as the percentage of transport in AdiC proteoliposomes in the absence of inhibitors. Data are from four to six experiments with three replicates per condition.

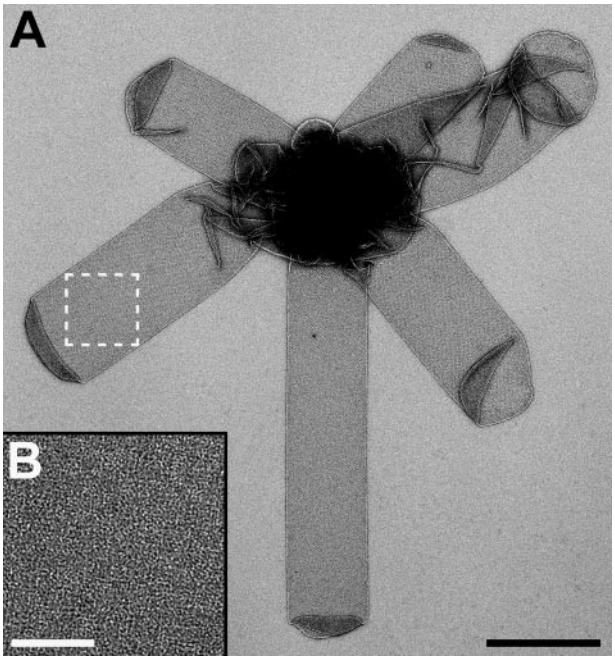

FIGURE 5. **TEM of negatively stained two-dimensional crystals of AdiC-W293L.** *A*, overview electron micrograph of tubular AdiC-W293L crystals. The area marked by the *white dashed box* was magnified and is displayed in *panel B*. The *scale bars* represent 0.6 μm (*A*) and 0.15 μm (*B*).

TABLE 1
Electron crystallographic data and statistics

Plane group symmetry	$p22_12_1$
Unit cell dimensions	a = 184 Å, b = 119 Å, γ = 90°
Number of processed electron micrographs	5
Resolution limit for merging	6.5 Å
Total number of observed reflections (index of quality ≤ 5)	1407
Number of unique reflections	981 (200 − 5 Å)/680 (200 − 6.5 Å)
Weighted phase error[a]	25.9° (200 − 5 Å)/23.5° (200 − 6.5 Å)
	16.0° (200 − 15.8 Å)
	24.5° (15.8 − 11.2 Å)
	20.3° (11.2 − 9.1 Å)
	33.7° (9.1 − 7.9 Å)
	36.5° (7.9 − 7.1 Å)
	35.3° (7.1 − 6.5 Å)
	54.6° (6.5 − 6.0 Å)
	37.9° (6.0 − 5.6 Å)
	49.7° (5.6 − 5.3 Å)
	52.2° (5.3 − 5.0 Å)

[a] Weighted phase error relative to the averaged and symmetrized dataset.

Table 1 for statistics). The unit cell, which harbored four AdiC dimers, had dimensions of a = 184 Å, b = 119 Å, γ = 90°, and a crystallographic $p22_12_1$ symmetry. As visible in Fig. 6*A*, two-dimensional crystals consisted of horizontal, alternating rows of up- and down-oriented AdiC-W293L dimers (up oriented dimers are mirror images of down oriented dimers and vice versa). Therefore, two-dimensional AdiC-W293L crystals

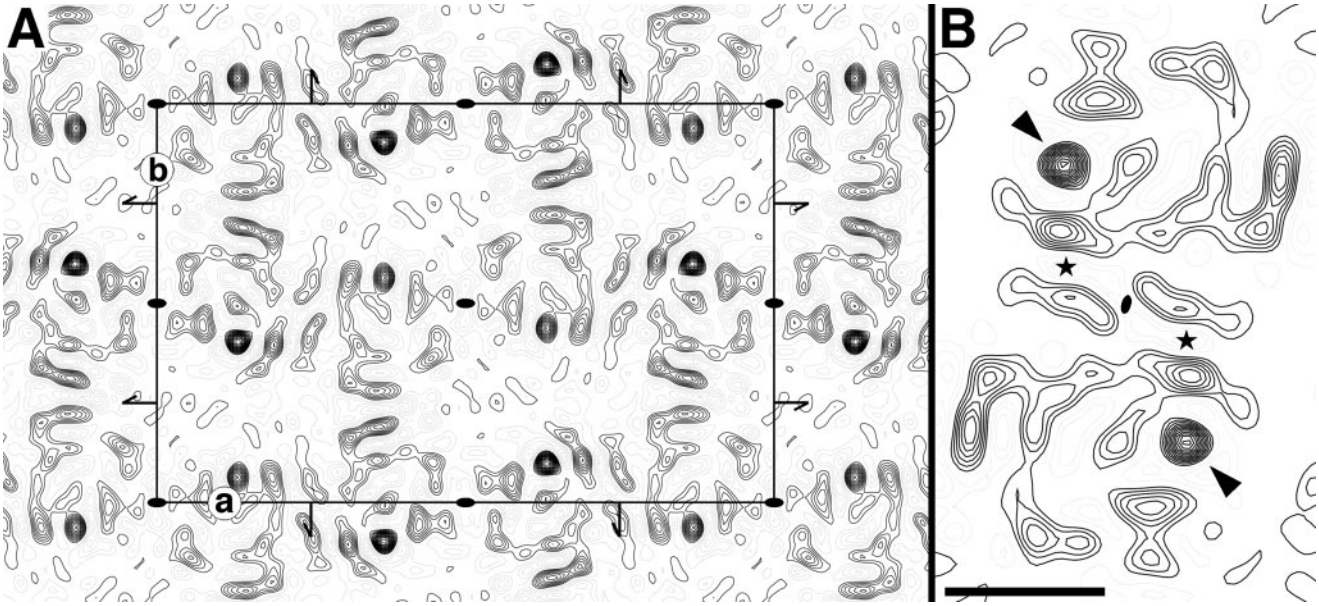

FIGURE 6. **Projection structure of AdiC-W293L.** *A*, $p22_12_1$-symmetrized projection map of AdiC-W293L at 6.5 Å resolution calculated from five electron micrographs. The *black rectangle* marks the unit cell (lattice dimensions: $a = 184$ Å, $b = 119$ Å, $\gamma = 90°$), which contains four AdiC-W293L dimers (two up- and two down-oriented dimers). *B*, improved projection map of AdiC-W293L after symmetrization of one of the four identical dimers in the unit cell exploiting the internal, non-crystallographic 2-fold symmetry axis of the dimer. The only strong density peak in the projection structure of the AdiC-W293L monomers is marked by *arrowheads*. The putative intradimeric contact sites are indicated by *stars*. The 2-fold axes perpendicular to the membrane plane and the screw axes parallel to the membrane plane are indicated. *Solid lines* indicate density above the mean, whereas negative contours are shown as *light gray lines*. The *scale bar* represents 25 Å.

expose both protein surfaces, *i.e.* the cytoplasmic and periplasmic side. To improve the projection structure of AdiC-W293L, one of the four identical dimers of the unit cell was symmetrized, exploiting the internal, non-crystallographic 2-fold symmetry axis of the dimer. This further improved the quality of the projection map as documented in Fig. 6*B*.

The overall shape of the AdiC-W293L dimer in two-dimensional crystals was elliptical with dimensions of ~95 × ~55 Å. From the 10–12 density peaks in the projection structure of the AdiC-W293L monomer, most of the densities were elongated with the exception of one single strong density peak (Fig. 6*B*, *arrowheads*).

DISCUSSION

From the literature, the origin of the AdiC protein is unclear, as it has been reported to belong to two groups of membrane transporters: the MFS (5, 7) and the APC superfamily (6). A *de novo* analysis of the phylogenetic relationship of AdiC with known transport proteins clearly indicated that AdiC belongs to the APC superfamily (Fig. 1). To elucidate the structure of membrane transporters from the APC superfamily using two-dimensional crystals and cryo-TEM, we cloned, overexpressed, purified, and biochemically and functionally characterized wild-type AdiC and the point mutant AdiC-W293L. For two-dimensional crystallization, overexpression of AdiC and AdiC-W293L yielded large quantities of pure protein (Fig. 2, *A* and *C*), *i.e.* 1–3 mg per liter of bacterial cell culture. BN-PAGE of purified AdiC and AdiC-W293L indicated an apparent molecular mass between 140 and 160 kDa, depending on the experimental conditions. Assuming an average mass of ~48.5 kDa for both AdiC forms and a DDM/Coomassie Brilliant Blue G-250 micelle of ~45 kDa bound to the proteins during BN-PAGE (36), AdiC and AdiC-W293L exist as dimers when solubilized in DDM. The latter was supported by TEM of negatively stained AdiC and AdiC-W293L proteins that showed elongated particles resembling two connected rings (Fig. 3, *B* and *C*). Furthermore, the elliptical shape of AdiC with dimensions of ~120 × ~75 Å is about twice as long as that of detergent-solubilized SteT monomers (SteT is also a member of the APC superfamily), which have dimensions of ~70 × ~60 Å (23). Interestingly, also the overall low resolution structures of SteT and AdiC monomers are similar, round-shaped with a central indentation. Finally, our results on the dimeric nature of AdiC are in line with a recent report by Fang *et al.* (5).

Reconstitution of AdiC into proteoliposomes confirmed the L-arginine/agmatine exchanger activity of the transporter (Fig. 4, *A* and *B*) and indicated relevant substrate recognition similarities to PotE. Thus, in both transporters the inhibition competence of substrate analogs depends on the size of the aliphatic chain connecting the two primary amino groups: cadaverine > putrescine > 1,3-diaminopropane in AdiC (Fig. 4*C*) and putrescine > 1,3-diaminopropane in PotE (35). In PotE the mutation W292L abolishes the transport activity of the protein (35). The same was the case for AdiC when introducing the corresponding point mutation, *i.e.* W293L (Fig. 4*B*). ITC of AdiC and AdiC-W293L showed the lack of substrate binding in the latter, demonstrating the role of the Trp-293 residue in substrate recognition. These data together with the close proximity to the substrate binding site or the permeation pathway of residue Cys-327 in the LAT transporter xCT (37) highlights the role of the putative transmembrane 8 in the substrate recognition of APC transporters.

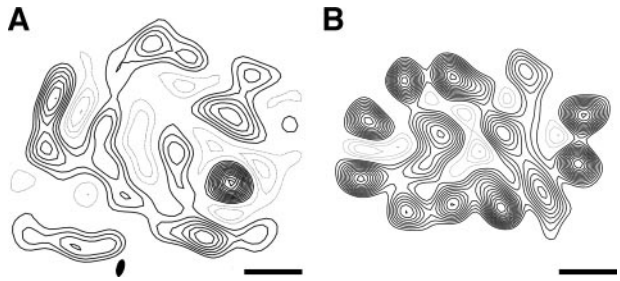

FIGURE 7. **Comparison of the AdiC-W293L and OxlT projection structures.** *A*, projection map of the putative AdiC-W293L monomer at a resolution of 6.5 Å, a member of the APC transporters superfamily. The internal, non-crystallographic 2-fold symmetry axis of the AdiC-W293L dimer is indicated. *B*, projection map of the OxlT monomer at 6 Å resolution (43), a member of the MFS. *Solid lines* indicate density above the mean, whereas *negative contours* are shown as *light gray lines*. The *scale bar* represents 10 Å.

The high amounts of pure and homogeneous protein formed an excellent basis for the two-dimensional crystallization of AdiC and AdiC-W293L. Both AdiC proteins had the propensity to form two-dimensional crystals. However, AdiC-W293L two-dimensional crystals were much more reproducible and better ordered, diffracting beyond 6 Å resolution. Similar to the lactose permease mutant LacY-C154G (38), the introduction of a single point mutation in AdiC, *i.e.* AdiC-W293L, improved the crystal quality and reproducibility considerably compared with wild-type AdiC crystals. Therefore, we focused on the determination of the projection structure of AdiC-W293L.

Cryo-TEM of two-dimensional AdiC-W293L crystals yielded the first detailed structure in projection of a transport protein from the APC superfamily. Reconstituted AdiC-W293L dimers were elliptical with dimensions of ~95 × ~55 Å. These dimensions are smaller than those of negatively stained detergent-solubilized AdiC particles (dimensions: ~120 × ~75 Å; see Fig. 3). Such differences are common because with detergent-solubilized membrane proteins dimensions are overestimated due to the bound detergent micelle, *e.g.* the aquaporin PM28A (SoPIP2;1): ~65 x ~65 Å in two-dimensional crystals (39) and ~95 x ~95 Å when solubilized in detergent (40). Although the exact number of transmembrane helices and their relative orientations within the molecule cannot be determined from the projection structure of AdiC-W293L, meaningful information is gained when compared with known membrane protein structures. For instance, the elongated density peaks suggest that the fold of AdiC consists mainly of tilted helices with the exception of one single strong density peak (Fig. 6*B*, *arrowheads*), which suggests a perpendicular membrane spanning α-helix. This is based on the projection and three-dimensional structures of aquaporins (41) and bacteriorhodopsin (42) that mainly consist of tilted or vertical transmembrane helices, respectively. As mentioned above, it is unclear from the literature if AdiC belongs to the MFS or APC superfamily. To verify our results from phylogenetic analysis (Fig. 1), indicating that AdiC is a member of the APC superfamily, we compared our AdiC projection structure with that of the oxalate/formate antiporter from *O. formigenes* (OxlT). OxlT is a typical 12-transmembrane helix transport protein from the MFS (43) (Fig. 7*B*), and the molecular mass is comparable with that of AdiC. The difference of the projection structure of the two proteins is striking, supporting the notion that AdiC does not belong to the MFS. Interestingly, the packing of the structural elements in OxlT is dense in contrast to AdiC. This is also reflected in the protein density area in the projection map of AdiC, which is distinctly larger than that of OxlT (Fig. 7). This difference between AdiC and OxlT explains the larger diameter measured for functional SteT (diameter, 7.4 nm; SteT is an APC family member) than for LacY (diameter, 6.0 nm; LacY is a MFS member) in reconstituted proteoliposomes (23). The OxlT monomer contains a near-2-fold symmetry that is evident in the projection map (Fig. 7*B*), relating two sets of six membrane-spanning helices, consistent with the clear homology between the first six and last six transmembrane segments in MFS transporters (43). This near-2-fold symmetry is not present in the putative AdiC-W293L monomer (Fig. 7*A*). In summary, we predict based on this comparison a markedly different structure for APC family members compared with transporter proteins from the MFS.

Acknowledgments—We are thankful to Teruhisa Hirai and Sriram Subramaniam for providing the projection structure of OxlT and to Susanna Bial for technical assistance in preparing E. coli membranes expressing the AdiC protein versions used.

REFERENCES

1. Donnenberg, M. S. (2000) *Nature* **406,** 768–774
2. Foster, J. W. (2004) *Nat. Rev. Microbiol.* **2,** 898–907
3. Gong, S., Richard, H., and Foster, J. W. (2003) *J. Bacteriol.* **185,** 4402–4409
4. Iyer, R., Williams, C., and Miller, C. (2003) *J. Bacteriol.* **185,** 6556–6561
5. Fang, Y., Kolmakova-Partensky, L., and Miller, C. (2007) *J. Biol. Chem.* **282,** 176–182
6. Jack, D. L., Paulsen, I. T., and Saier, M. H., Jr. (2000) *Microbiology* **146,** 1797–1814
7. Saier, M. H., Jr., Beatty, J. T., Goffeau, A., Harley, K. T., Heijne, W. H., Huang, S. C., Jack, D. L., Jahn, P. S., Lew, K., Liu, J., Pao, S. S., Paulsen, I. T., Tseng, T. T., and Virk, P. S. (1999) *J. Mol. Microbiol. Biotechnol.* **1,** 257–279
8. Hu, L. A., and King, S. C. (1998) *Biochem. J.* **336,** 69–76
9. Ellis, J., Carlin, A., Steffes, C., Wu, J., Liu, J., and Rosen, B. P. (1995) *Microbiology* **141,** 1927–1935
10. Cosgriff, A. J., and Pittard, A. J. (1997) *J. Bacteriol.* **179,** 3317–3323
11. Gasol, E., Jimenez-Vidal, M., Chillaron, J., Zorzano, A., and Palacin, M. (2004) *J. Biol. Chem.* **279,** 31228–31236
12. Nicholson, B., Manner, C. K., Kleeman, J., and MacLeod, C. L. (2001) *J. Biol. Chem.* **276,** 15881–15885
13. Yeramian, A., Martin, L., Serrat, N., Arpa, L., Soler, C., Bertran, J., McLeod, C., Palacin, M., Modolell, M., Lloberas, J., and Celada, A. (2006) *J. Immunol.* **176,** 5918–5924
14. Yeramian, A., Martin, L., Arpa, L., Bertran, J., Soler, C., McLeod, C., Modolell, M., Palacin, M., Lloberas, J., and Celada, A. (2006) *Eur. J. Immunol.* **36,** 1516–1526
15. Fuchs, B. C., and Bode, B. P. (2005) *Semin. Cancer Biol.* **15,** 254–266
16. Calonge, M. J., Gasparini, P., Chillaron, J., Chillon, M., Gallucci, M., Rousaud, F., Zelante, L., Testar, X., Dallapiccola, B., Di Silverio, F., Barcelo, P., Estivill, X., Zorzano, A., Nunes, A., and Palacin, M. (1994) *Nat. Genet.* **6,** 420–425
17. Feliubadalo, L., Font, M., Purroy, J., Rousaud, F., Estivill, X., Nunes, V., Golomb, E., Centola, M., Aksentijevich, I., Kreiss, Y., Goldman, B., Pras, M., Kastner, D. L., Pras, E., Gasparini, P., Bisceglia, L., Beccia, E., Gallucci, M., de Sanctis, L., Ponzone, A., Rizzoni, G. F., Zelante, L., Bassi, M. T., George, A. L., Jr., Manzoni, M., De Grandi, A., Riboni, M., Endsley, J. K.,

Ballabio, A., Borsani, G., Reig, N., Fernandez, E., Estevez, R., Pineda, M., Torrents, D., Camps, M., Lloberas, J., Zorzano, A., and Palacin, M. (1999) *Nat. Genet.* **23,** 52–57
18. Torrents, D., Mykkanen, J., Pineda, M., Feliubadalo, L., Estevez, R., de Cid, R., Sanjurjo, P., Zorzano, A., Nunes, V., Huoponen, K., Reinikainen, A., Simell, O., Savontaus, M. L., Aula, P., and Palacin, M. (1999) *Nat. Genet.* **21,** 293–296
19. Borsani, G., Bassi, M. T., Sperandeo, M. P., De Grandi, A., Buoninconti, A., Riboni, M., Manzoni, M., Incerti, B., Pepe, A., Andria, G., Ballabio, A., and Sebastio, G. (1999) *Nat. Genet.* **21,** 297–301
20. Kaleeba, J. A., and Berger, E. A. (2006) *Science* **311,** 1921–1924
21. Yernool, D., Boudker, O., Jin, Y., and Gouaux, E. (2004) *Nature* **431,** 811–818
22. Yamashita, A., Singh, S. K., Kawate, T., Jin, Y., and Gouaux, E. (2005) *Nature* **437,** 215–223
23. Reig, N., del Rio, C., Casagrande, F., Ratera, M., Gelpi, J. L., Torrents, D., Henderson, P. J., Xie, H., Baldwin, S. A., Zorzano, A., Fotiadis, D., and Palacin, M. (2007) *J. Biol. Chem.* **282,** 13270–13281
24. Stahlberg, H., Fotiadis, D., Scheuring, S., Remigy, H., Braun, T., Mitsuoka, K., Fujiyoshi, Y., and Engel, A. (2001) *FEBS Lett.* **504,** 166–172
25. Raunser, S., Appel, M., Ganea, C., Geldmacher-Kaufer, U., Fendler, K., and Kuhlbrandt, W. (2006) *Biochemistry* **45,** 12796–12805
26. Do, C. B., Mahabhashyam, M. S., Brudno, M., and Batzoglou, S. (2005) *Genome Res.* **15,** 330–340
27. Huelsenbeck, J. P., and Ronquist, F. (2001) *Bioinformatics* **17,** 754–755
28. Letunic, I., and Bork, P. (2007) *Bioinformatics* **23,** 127–128
29. Xie, H., Patching, S. G., Gallagher, M. P., Litherland, G. J., Brough, A. R., Venter, H., Yao, S. Y., Ng, A. M., Young, J. D., Herbert, R. B., Henderson, P. J., and Baldwin, S. A. (2004) *Mol. Membr. Biol.* **21,** 323–336
30. Schägger, H., and von Jagow, G. (1991) *Anal. Biochem.* **199,** 223–231
31. Hirai, T., Murata, K., Mitsuoka, K., Kimura, Y., and Fujiyoshi, Y. (1999) *J. Electron Microsc.* (*Tokyo*) **48,** 653–658
32. Philippsen, A., Schenk, A. D., Signorell, G. A., Mariani, V., Berneche, S., and Engel, A. (2007) *J. Struct. Biol.* **157,** 28–37
33. Philippsen, A., Schenk, A. D., Stahlberg, H., and Engel, A. (2003) *J. Struct. Biol.* **144,** 4–12
34. Valpuesta, J. M., Carrascosa, J. L., and Henderson, R. (1994) *J. Mol. Biol.* **240,** 281–287
35. Kashiwagi, K., Kuraishi, A., Tomitori, H., Igarashi, A., Nishimura, K., Shirahata, A., and Igarashi, K. (2000) *J. Biol. Chem.* **275,** 36007–36012
36. Suda, K., Filipek, S., Palczewski, K., Engel, A., and Fotiadis, D. (2004) *Mol. Membr. Biol.* **21,** 435–446
37. Jimenez-Vidal, M., Gasol, E., Zorzano, A., Nunes, V., Palacin, M., and Chillaron, J. (2004) *J. Biol. Chem.* **279,** 11214–11221
38. Abramson, J., Smirnova, I., Kasho, V., Verner, G., Kaback, H. R., and Iwata, S. (2003) *Science* **301,** 610–615
39. Kukulski, W., Schenk, A. D., Johanson, U., Braun, T., de Groot, B. L., Fotiadis, D., Kjellbom, P., and Engel, A. (2005) *J. Mol. Biol.* **350,** 611–616
40. Karlsson, M., Fotiadis, D., Sjovall, S., Johansson, I., Hedfalk, K., Engel, A., and Kjellbom, P. (2003) *FEBS Lett.* **537,** 68–72
41. Engel, A., Fujiyoshi, Y., and Agre, P. (2000) *EMBO J.* **19,** 800–806
42. Subramaniam, S., Hirai, T., and Henderson, R. (2002) *Philos. Transact. A Math. Phys. Eng.* **360,** 859–874
43. Heymann, J. A., Sarker, R., Hirai, T., Shi, D., Milne, J. L., Maloney, P. C., and Subramaniam, S. (2001) *EMBO J.* **20,** 4408–4413